DOI:
10.1016/j.jsb.2017.10.004

Document Version
Peer reviewed version

Technical Note

Online Raman spectroscopy for Structural Biology on beamline ID29 of the ESRF

David von Stetten, Thierry Giraud, Soi Bui, Roberto A. Steiner, François Fihman, Daniele de Sanctis, Antoine Royant

PII: S1047-8477(17)30172-7
DOI: https://doi.org/10.1016/j.jsb.2017.10.004
Reference: YJSBI 7109

To appear in: *Journal of Structural Biology*

Received Date: 20 July 2017
Revised Date: 11 October 2017
Accepted Date: 13 October 2017

Please cite this article as: von Stetten, D., Giraud, T., Bui, S., Steiner, R.A., Fihman, F., de Sanctis, D., Royant, A., Online Raman spectroscopy for Structural Biology on beamline ID29 of the ESRF, *Journal of Structural Biology* (2017), doi: https://doi.org/10.1016/j.jsb.2017.10.004

Technical Note

Online Raman spectroscopy for Structural Biology on beamline ID29 of the ESRF

David von Stetten[a,*], Thierry Giraud[a], Soi Bui[b], Roberto A. Steiner[b], François Fihman[c], Daniele de Sanctis[a,*], Antoine Royant[a,d,*]

[a]European Synchrotron Radiation Facility (ESRF), F-38043 Grenoble, France

[b]Randall Division of Cell and Molecular Biophysics, King's College London, London SE1 1UL, UK

[c]6tec, 745 route de Grenoble, F-38260 La Frette, France

[d]Univ. Grenoble Alpes, CNRS, CEA, IBS (Institut de Biologie Structurale), F-38000 Grenoble, France

[*]Corresponding authors.

E-mail addresses: david.von_stetten@esrf.fr (D. von Stetten), daniele.de_sanctis@esrf.fr (D. de Sanctis), antoine.royant@ibs.fr (A. Royant).

Abstract

Raman spectroscopy can probe the structure and conformations of specific chemical groups within proteins and may thus be used as a technique complementary to X-ray crystallography. This combined approach can be decisive in resolving ambiguities in the interpretation of enzymatic or X-ray induced processes. Here, we present an online Raman setup developed at the European Synchrotron that allows for interleaved Raman spectra acquisition and X-ray diffraction measurements with fast probe exchange and simple alignment while maintaining a high sensitivity over the entire spectral range. This device has been recently employed in the study of a covalent intermediate in the O_2-dependent breakdown of uric acid by the cofactor-free enzyme urate oxidase and to monitor its decay induced by X-ray exposure.

Keywords: Raman spectroscopy, macromolecular crystallography, diffraction-complementary technique, kinetic crystallography, radiation damage.

1. Introduction

The use of non-resonant Raman spectroscopy on protein crystals has been pioneered by the group of Paul Carey using Raman microscopes on enzyme crystals in their mother liquor at room temperature (Carey and Dong, 2004). While Raman spectra of proteins are complex, the calculation of time-dependent difference spectra removes the vast majority of protein vibrational modes and unmasks a few protein- and ligand-specific modes associated with the enzymatic reaction, providing insights on their mechanism. The method has been coined 'Raman crystallography' (Carey et al., 2011), and could help identify the formation of a *trans*-enamine species in the inhibition mechanism of a -lactamase by various clinical inhibitors (Helfand et al., 2003) or follow chain extension by a DNA polymerase (Espinosa-Herrera et al., 2013). Besides proteins, other complex biomolecules such as nucleic acids can also be studied by Raman crystallography, for instance to provide the pKa of the catalytic base from a ribozyme (Gong et al., 2007).

Following up on these developments, the group of Dominique Bourgeois postulated that Raman spectroscopy could be used for kinetic crystallography purposes as a monitor of the progress of a reaction occurring *in crystallo* (Bourgeois & Royant, 2005) *via* the changes in specific modes so that various intermediates could be trapped by timely flash-cooling in liquid nitrogen. With this idea in mind, they managed to prove that the key intermediate in the reaction mechanism of superoxide oxidase was an end-on peroxide species (Katona et al., 2007). This use of Raman spectroscopy as a preparative way for diffraction experiments was then coined 'Raman-assisted crystallography' (RaX). It was soon realized that RaX, if directly used on a X-ray beamline diffractometer (in the so-called 'online' mode (Carpentier et al., 2007), could be used as a metric of specific radiation damage to certain covalent bonds within biomolecules, namely their breakage (Burmeister, 2000; Ravelli and McSweeney, 2000; Weik et al., 2000). The first online setup was installed on the ESRF Structural Biology beamline ID14-2 (Wakatsuki et al., 1998), then on beamline ID23-1 (Nurizzo et al., 2006). It was used to visualize the X-ray induced breakage of C-Br bonds in brominated DNA (McGeehan et al., 2007), disulphide bonds in lysozyme and insulin (Carpentier et al., 2010; McGeehan et al., 2011), and the loss of conjugation in a fluorescent chromophore (Adam et al., 2009). Similar setups were developed at the Swiss-Norwegian Beamline (SNBL) beamline BM01 at the ESRF (van Beek et al., 2011), which allowed for the visualization of the one-electron-

induced loss of planarity of a flavin cofactor (Røhr et al., 2010), and at the Swiss Light Source (Pompidor et al., 2013), that led to the elucidation of how NO molecules are selectively photodissociated from haems by X-rays in haemoglobin crystals (Merlino et al., 2013). Another setup used to be available at the National Synchrotron Light Source (NSLS) facility at Brookhaven National Laboratory (Stoner-Ma *et al.*, 2011) until its closure in 2014.

An important issue when performing on-line spectroscopy measurements is to make sure that the laser probes a volume contained within the one that was irradiated by X-rays, particularly when investigating the effects of radiation damage. For this reason, we have designed a new Raman probe support in on-axis geometry (*i.e.*, with the Raman laser coaxial to the X-ray beam) on beamline ID29 (de Sanctis et al., 2012), which uses, *via* optical fibres, the Raman spectrometer on ID29S (von Stetten et al., 2015). The on-axis geometry greatly facilitates the alignment of the laser probe onto the X-ray beam location and ensures that X-ray diffraction data and Raman spectra are recorded from the same sample volume.

2. Instrument description

A motorized head support fitting an InVia Raman probe (Renishaw, Wotton-under-Edge, United Kingdom) was designed and built. Three different InVia probes are available, corresponding to the three excitation lasers: 532 nm (green), 633 nm (red) and 785 nm (near-infrared). The support consists of a two-translation stage to which a third linear vertical stage is orthogonally attached (Fig. 1), allowing translation along three directions: one that is parallel to the X-ray beam (*X*, pointing from the X-ray source to the sample), a second one horizontal (*Y*, pointing outboard), and one vertical (*Z*, pointing upward). The probe is attached to the vertical stage and is coupled via a 45° mirror to a 50x objective (Leica, N Plan class, L 50x/0.50) that focuses the laser beam along the X-ray beam direction on a focal volume of 20 x 20 x 40 μm^3 at a working distance of 8.3 mm (Carpentier et al., 2007). Translations along *Y* and *Z* are used to align the laser on the sample and adjustment along *X* allows for focusing the laser focal spot on the crystal surface. Movements in the three directions are performed *via* endless screws coupled to stepper motors. The translation ranges are 15 mm along *X*, 10 mm along *Y*, and 7 mm along *Z* with a motor precision lower than 1 µm. All motors are driven by IcePAP controllers and can be moved either directly *via* the IcePAP interface or the beamline BLISS control software

(http://gitlab.esrf.fr/bliss/bliss). The focal spot of the laser can be aligned to the X-ray beam position by moving these motors while monitoring the laser position in the MxCuBE GUI (Gabadinho et al., 2010) through the On Axis Viewer (OAV) microscope, after shifting the crystal sideways out of the beam path. Alternatively the fluorescence screen of the MD2 diffractometer (Arinax, Voreppe, France) can be used to visualize and optimize the focus of the laser at the sample position.

The Raman head is secured in two stable positions, '*in*' and '*out*', with a hinge locking mechanism aligned parallel to the *Y* axis. Exchange between the two configurations is performed manually within a few minutes. In the '*out*' position (Fig. 1D), the device does not obstruct the X-ray beam, even at high diffraction angle, while the '*in*' position is used for Raman measurements (Fig. 1E). Small position corrections (~10 μm) are required after switching to the '*in*' mode. The support is secured on the diffractometer frame at two places: on the back frame, close to the pivoting hinge and on the inboard frame, on the female thread designed for the lifting hook.

Operation of the Raman on line experiments is protected by the Personal Safety System (PSS). The ESRF X-ray Personal Safety System ensures that no user is present inside the experimental hutch when the hutch door is interlocked, and thus authorises the opening of the X-ray shutters. An additional laser PSS permits to safely operate lasers inside the experimental hutch. This might be either a locally installed laser or, in the case of ID29, one of the three Raman lasers that is connected via a 50 m-long optical fibre from the adjacent hutch of ID29S (also known as 'Cryobench' (von Stetten et al., 2015)), where the Raman spectrometer is located. Therefore, the ID29 and ID29S PSS are linked to allow the simultaneous operation of the Raman spectrophotometer (inside the ID29S laboratory) and of the fibre-connected Raman probe (inside the ID29 Experimental Hutch). The PSSs of the two experimental hutches have been made interdependent such that breaking the interlock of any of the two experimental hutches closes the safety shutter of the Raman laser. However, unlike the ESRF X-ray PSS, the laser PSS can be overridden and allows for the presence of expert users, wearing protective equipment such as laser goggles, in the experimental hutch. This mode can be used to manually intervene in the experimental hutch while the laser is on.

Remarkably, the insertion of a 50-m long fibre in-between the Raman spectrometer located in ID29S and the probe present in ID29 only results in a ~50% loss of the

excitation light power at the sample position when compared to the situation when the probe is used in ID29S (25 mW *vs.* 50 mW), and the same on the way back, which means that the intensities of spectra recorded with the online setup are decreased fourfold compared to offline ones. An interpretable Raman spectrum is typically recorded in a few minutes, while spectra with longer accumulation time (typically 30 min) may be necessary to reveal fine details of the Raman peaks.

3. Example of biological application

In order to demonstrate the sensitivity of our setup, we have used it on a challenging project aimed at monitoring the X-ray induced breakage of a bond with a weak Raman signature. Urate oxidase (UOX) is a cofactor-independent oxidase (Fetzner and Steiner, 2010) that catalyses the O_2-dependent breakdown of uric acid to 5-hydroxyisourate following a mechanism that has been proposed to involve a peroxide adduct (Kahn and Tipton, 1998). Peroxide intermediates are formed in many biological reactions involving molecular oxygen. However, their structural determination is difficult as these compounds are often not very stable. We have combined high-resolution crystallography and Raman spectroscopy to unambiguously demonstrate the presence of such a peroxide intermediate, and the structure thereof, in the reaction mechanism of urate oxidase. While the mechanistic implications of this structure have already been published (Bui et al., 2014), we focus here on the experimental details. The crystallisation in presence of 9-methyl uric acid as substrate analogue allowed the identification of a low-intensity peroxide-specific Raman band at 605 cm^{-1}, which was further confirmed by ^{18}O isotope labelling and QM/MM calculations (Bui et al., 2014). A crystal of urate oxidase prepared in conditions leading to the formation of the peroxide intermediate was chosen to be of maximal size (450 x 450 x 450 μm^3, significantly larger than the X-ray beam of 50 x 30 μm^2 Gaussian shape) to maximize diffraction (up to 1.3 Å) while being able to deposit X-ray doses as low as 2.5 kGy (Zeldin et al., 2013) during 7 successive data collections performed at 100 K, while 5 data collections of increased doses (12.5 to 184 kGy) were inserted as 'burn' data collections to probe the logarithmic behaviour of the damage mechanism. All X-ray data sets were collected from the same 180° wedge. Raman spectra (2000 s acquisition time, 200 cm^{-1} – 1800 cm^{-1} spectral range) were recorded using the 785 nm laser probe in-between each sequence of structural and burn data collections.

Because the crystal was larger than the beam, the on-axis geometry was crucial to ensure that only an X-ray irradiated volume of the crystal was probed by the Raman laser. However, X-ray crystallography and Raman spectroscopy differentially probe the kinetics of X-ray damage because the X-ray data is averaged over a slice through the large crystal, while the Raman spectra originate from a shallow area on the surface of the crystal (20x20 μm², with about 40 μm penetration depth) that was only transiently irradiated during the X-ray data collection. Thanks to the on-axis geometry, this Raman-probed part is within the X-ray irradiated slice, but X-ray crystallography and Raman spectroscopy probe radiation damage to urate oxidase on different dose scales (up to ~700 kGy *vs.* ~200 kGy). Yet, the overlap of dose points observed by each technique allows for the comparison of both types of experimental data. We were thus able to monitor the structural and kinetic details the progressive disappearance of the peroxide intermediate on a fast dose scale (half-dose of 88 kGy^{-1}) by the rupture of the C_5-Op1 bond (Fig. 2A) that is correlated to the decay of the weak 605 cm^{-1} Raman band (Fig. 2B and C). Thanks to the quality of both the structural and Raman data, the observed decays could be best modelled by a biexponential curve and rationalized assuming a pathway of X-ray induced peroxide regeneration acting alongside its decomposition, which provided important information on the enzymatic mechanism of urate oxidase (Bui et al., 2014; Bui and Steiner, 2016).

4. Conclusion

The analysis of Raman spectra of protein crystals helps with the interpretation of X-ray data and can elucidate structural details that cannot be deduced from X-ray diffraction measurements alone. With the new Raman support presented here, recording Raman spectra on ID29 is readily available and can be done while the sample is mounted on the diffractometer, therefore allowing to optimally correlate X-ray and Raman data without the need to transfer the sample. More recently, the same setup has also been used to visualize how the chromophore of the fluorescent protein mNeonGreen is protonated and loses conjugation upon X-ray irradiation (Clavel et al., 2016). Finally, the motorised support could be used to accommodate other probes used in the back-scattering geometry, for instance to record emission fluorescence spectra or to deliver actinic light onto the sample. When feasible, we advocate that *in crystallo* spectroscopic techniques should always be used in conjunction with

crystallographic studies as they often provide orthogonal information that can enhance the mechanistic understanding of the process under investigation. Our urate oxidase results show how the structure elucidation of a key covalent intermediate could have been missed by recording diffraction data collections depositing on the crystal the routine dose of 100 kGy. Similarly, *in crystallo* Raman spectroscopy was instrumental in proving the presence of a peroxo intermediate in the reaction of superoxide reductase, in the end-on conformation, whose covalent bond could have been missed in the 1.95 Å resolution electron density (Katona et al., 2007).

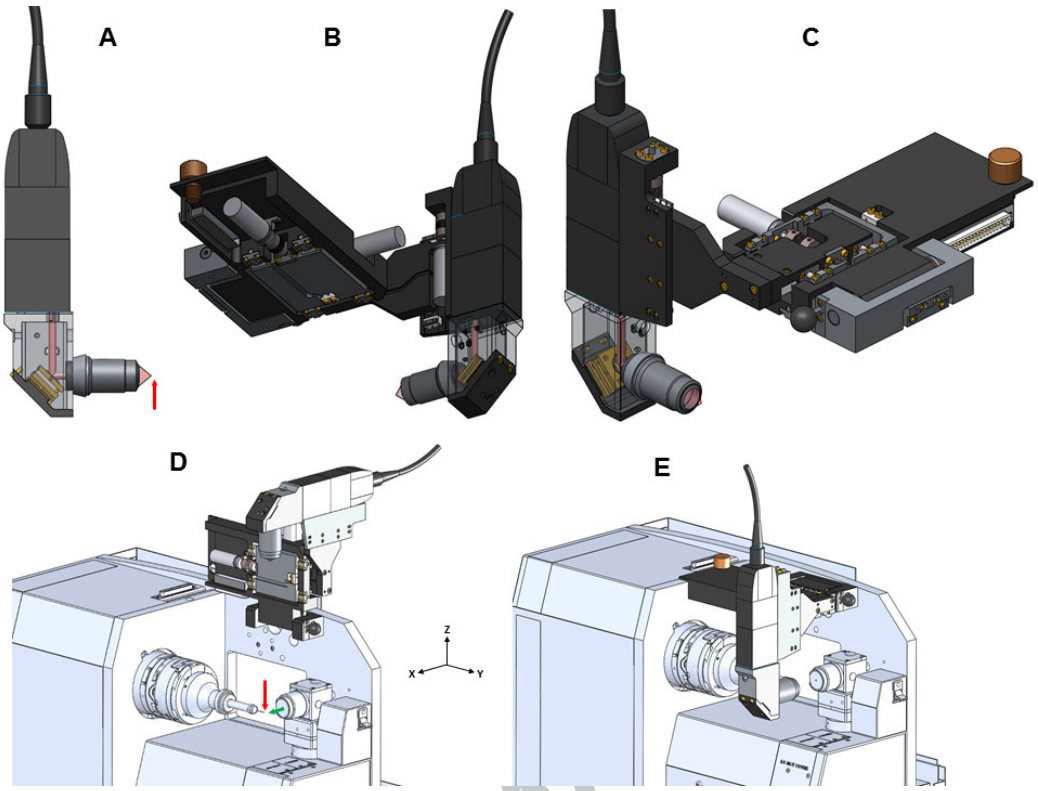

Fig. 1. Online Raman setup on beamline ID29. (A) Renishaw InVia Raman head with an added 45° mirror (B, C) Motorized Raman head support from two different orientations (D) '*Out*' position, allowing for X-ray data collection. (E) '*In*' position, allowing for Raman data collection. The (*X*, *Y*, *Z*) referential for the lower panels correspond to the X-ray path (*X*), the diffractometer rotation axis (*Y*) and the vertical line (*Z*). Red arrows point at the sample position. The green arrow indicates the X-ray path after the On-Axis Viewer.

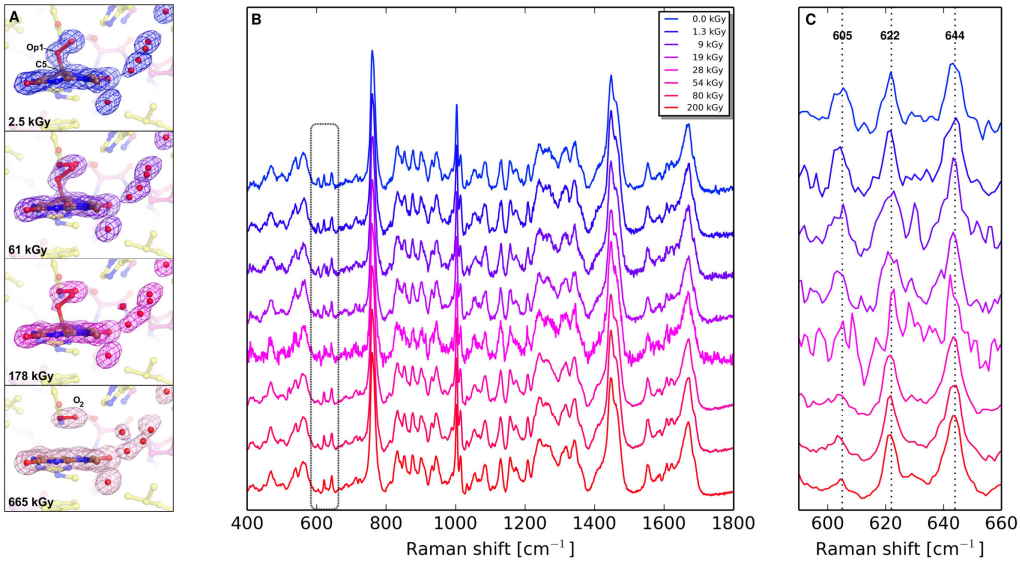

Fig. 2. Correlated structural and Raman analysis of radiation damage to a peroxide intermediate of urate oxidase (Bui et al., 2014). (A) X-ray structures at increasing doses showing the progressive rupture of the C_5-Op1 bond, which is accompanied by the loss of pyramidalization at C_5, leading to a planar structure and the release of dioxygen. (B) Raman spectra of UOX crystal after increasing X-ray exposure. (C) Close-up on the spectral region around the X-ray sensitive 605 cm^{-1} Raman band.

Acknowledgements

The authors are acknowledging the ESRF for financial support and access to beamlines on the in-house research program, the ESRF Structural Biology group for their support, most particularly Hugo Caserotto and Fabien Dobias for helpful advice during the design, commissioning and use of this device. The authors also acknowledge the platforms of the Grenoble Instruct center (ISBG; UMS 3518 CNRS-CEA-UJF-EMBL) supported by the French Infrastructure for Integrated Structural Biology Initiative FRISBI (ANR-10-INSB-05-02) and GRAL (ANR-10-LABX-49-01) within the Grenoble Partnership for Structural Biology (PSB).

References

Adam, V., Carpentier, P., Violot, S., Lelimousin, M., Darnault, C., Nienhaus, G. U., Bourgeois, D., 2009. Structural basis of X-ray-induced transient photobleaching in a photoactivatable green fluorescent protein. J. Am. Chem. Soc. 131, 18063–18065.

van Beek, W., Safonova, O. V., Wiker, G., Emerich, H., 2011. SNBL, a dedicated beamline for combined in situ X-ray diffraction, X-ray absorption and Raman scattering experiments. Phase Transit. 84, 726–732.

Bourgeois, D., Royant, A., 2005. Advances in kinetic protein crystallography. Curr. Opin. Struct. Biol. 15, 538-547.

Bui, S., Steiner, R. A., 2016. New insight into cofactor-free oxygenation from combined experimental and computational approaches. Curr. Opin. Struct. Biol. 41, 109–118.

Bui, S., von Stetten, D., Jambrina, P. G., Prangé, T., Colloc'h, N., de Sanctis, D., Royant, A., Rosta, E., Steiner, R. A. (2014). Direct evidence for a peroxide intermediate and a reactive enzyme-substrate-dioxygen configuration in a cofactor-free oxidase. Angew. Chem. Int. Ed. 53, 13710–13714.

Burmeister, W. P., 2000. Structural changes in a cryo-cooled protein crystal owing to radiation damage. Acta Crystallogr. D Biol. Crystallogr. 56, 328–341.

Carey, P. R., Chen, Y., Gong, B., Kalp, M., 2011. Kinetic crystallography by Raman microscopy. Biochim. Biophys. Acta 1814, 742-749.

Carey, P. R., Dong, J., 2004. Following ligand binding and ligand reactions in proteins via Raman crystallography. Biochemistry 43, 8885–8893.

Carpentier, P., Royant, A., Ohana, J., Bourgeois, D., 2007. Advances in spectroscopic methods for biological crystals. 2. Raman spectroscopyJ. Appl. Crystallogr. 40, 1113–1122.

Carpentier, P., Royant, A., Weik, M., Bourgeois, D., 2010. Raman-assisted crystallography suggests a mechanism of X-ray-induced disulfide radical formation and reparation. Structure. 18, 1410–1419.

Clavel, D., Gotthard, G., von Stetten, D., De Sanctis, D., Pasquier, H., Lambert, G. G., Shaner, N. C., Royant, A., 2016. Structural analysis of the bright monomeric yellow-green fluorescent protein mNeonGreen obtained by directed evolution. Acta Crystallogr. D Biol. Crystallogr. 72, 1298–1307.

Espinoza-Herrera, S. J., Gaur, V., Suo, Z., Carey, P. R., 2013. Following DNA chain extension and protein conformational changes in crystals of a Y-family DNA polymerase via Raman crystallography. Biochemistry 52, 4881-4890.

Fetzner, S., Steiner, R. A., 2010. Cofactor-independent oxidases and oxygenases. Appl. Microbiol. Biotechnol. 86, 791–804.

Gabadinho, J., Beteva, A., Guijarro, M., Rey-Bakaikoa, V., Spruce, D., et al., 2010. MxCuBE: a synchrotron beamline control environment customized for macromolecular crystallography experiments. J. Synchrotron Radiat. 17, 700-707.

M.Gong, B., Chen, J. H., Chase, E., Chadalavada, D. M., Yajima, R., Golden, B. L., Bevilacqua, P. C., Carey, P. R., 2007. Direct measurement of a pK(a) near neutrality for the catalytic cytosine in the genomic HDV ribozyme using Raman crystallography. J. Am. Chem. Soc. 129, 13335-13342.

Helfand, M. S., Totir, M. A., Carey, M. P., Hujer, A. M., Bonomo, R. A., Carey, P. R., 2003. Following the reactions of mechanism-based inhibitors with beta-lactamase by Raman crystallography. Biochemistry 42, 13386-13392.

Kahn, K., Tipton, P. A., 1998. Spectroscopic characterization of intermediates in the urate oxidase reaction. Biochemistry 37, 11651–11659.

Katona, G., Carpentier, P., Nivière, V., Amara, P., Adam, V., Ohana, J., Tsanov, N., Bourgeois, D., 2007. Raman-assisted crystallography reveals end-on peroxide intermediates in a nonheme iron enzyme. Science 316, 449-453.

McGeehan, J. E., Bourgeois, D., Royant, A., Carpentier, P., 2011. Raman-assisted crystallography of biomolecules at the synchrotron: instrumentation, methods and applications. Biochim. Biophys. Acta 1814, 750–759.

McGeehan, J. E., Carpentier, P., Royant, A., Bourgeois, D., Ravelli, R. B. G., 2007. X-ray radiation-induced damage in DNA monitored by online Raman. J. Synchrotron Radiat. 14, 99–108.

Merlino, A., Fuchs, M.R., Pica, A., Balsamo, A., Dworkowski, F.S., Pompidor, G., Mazzarella, L., Vergara, A., 2013. Selective X-ray-induced NO photodissociation in haemoglobin crystals: evidence from a Raman-assisted crystallographic study. Acta Crystallogr. D Biol. Crystallogr. 69, 137-140.

Nurizzo, D., Mairs, T., Guijarro, M., Rey, V., Meyer, J., Fajardo, P., Chavanne, J., Biasci, J.-C., McSweeney, S., Mitchell, E., 2006. The ID23-1 structural biology beamline at the ESRF. J. Synchrotron Rad. 13, 227-238.

Pompidor, G., Dworkowski, F. S. N., Thominet, V., Schulze-Briese, C., Fuchs, M. R., 2013. A new on-axis micro-spectrophotometer for combining Raman, fluorescence and UV/Vis absorption spectroscopy with macromolecular crystallography at the Swiss Light Source. J. Synchrotron Radiat. 20, 765–776.

Ravelli, R. B., McSweeney, S. M., 2000. The 'fingerprint' that X-rays can leave on structures. Structure 8, 315–328.

Røhr, A. K., Hersleth, H. P., Andersson, K. K., 2010. Tracking flavin conformations in protein crystal structures with Raman spectroscopy and QM/MM calculations. Angew. Chem. Int. Ed. 49, 2324–2327.

de Sanctis, D., Beteva, A., Caserotto, H., Dobias, F., Gabadinho, J., Giraud, T., Gobbo, A., Guijarro, M., Lentini, M., Lavault, B., Mairs, T., McSweeney, S., Petitdemange, S., Rey-Bakaikoa, V., Surr, J., Theveneau, P., Leonard, G. A., Mueller-Dieckmann, C., 2012. ID29: a high-intensity highly automated ESRF beamline for macromolecular crystallography experiments exploiting anomalous scattering. J. Synchrotron Radiat. 19, 455–461.

von Stetten, D., Giraud, T., Carpentier, P., Sever, F., Terrien, M., Dobias, F., Juers, D. H., Flot, D., Mueller-Dieckmann, C., Leonard, G. A., de Sanctis, D., Royant, A., 2015. *In crystallo* optical spectroscopy (icOS) as a complementary tool on the macromolecular crystallography beamlines of the ESRF. Acta Crystallogr. D Biol. Crystallogr. 71, 15–26.

Stoner-Ma, D., Skinner, J. M., Schneider, D. K., Cowan, M., Sweet, R. M., Orville, A. M., 2011. Single-crystal Raman spectroscopy and X-ray crystallography at beamline X26-C of the NSLS. J. Synchrotron Radiat. 18, 37–40.

Wakatsuki, S., Belrhali, H., Mitchell, E. P., Burmeister, W. P., McSweeney, S. M., Kahn, R., Bourgeois, D., Yao, M., Tomizaki, T, Theveneau, P., 1998. ID14 'Quadriga', a Beamline for Protein Crystallography at the ESRF. J. Synchrotron Rad. 5, 215–221.

Weik, M., Ravelli, R. B., Kryger, G., McSweeney, S., Raves, M. L., Harel, M., Gros, P., Silman, I., Kroon, J., Sussman, J. L., 2000. Specific chemical and structural damage to proteins produced by synchrotron radiation. Proc. Natl. Acad. Sci. USA 97, 623–628.

Zeldin, O. B., Gerstel, M., Garman, E. F., 2013. RADDOSE-3D: time- and space-resolved modelling of dose in macromolecular crystallography. J. Appl. Crystallogr. 46, 1225–1230.